Coupled Thermal-Mechanical Analysis of Power Electronic Modules with Finite Element Method and Parametric Model Order Reduction

Sheikh Hassan[a,*], Pushparajah Rajaguru[a], Stoyan Stoyanov[a], Christopher Bailey[b], Timothy Tilford[a]

[a]*School of Computing and Mathematical Sciences, University of Greenwich, Greenwich, London SE10 9LS, UK.*
[b]*School of Electrical, Computer and Energy Engineering, Arizona State University, Arizona, USA.*

Abstract

This work presents a new approach for performing a parametric study and examining nonlinear material behaviours of a coupled thermal-mechanical model of a Power Electronics Module (PEM) by integrating the Finite Element Method (ANSYS-FEM) with Parametric Model Order Reduction (pMOR). The considered coupling method solves the thermal and structural models concurrently compared to the widely practised sequential coupling method. Instead of constant parameter values, which are generally regarded for pMOR studies, the temperature-dependent material properties of the wire material have been parametrised in the work using the pMOR method. A generalised 2D model has been regarded here for thermal-mechanical analysis with the pMOR approach, parametrising temperature-dependent coefficient of thermal expansion (CTE) and Young's modulus (E) of the wire material to explore their impact on wire bonds. The matrix interpolation method has been applied here for the pMOR study, and PRIMA, a Krylov subspace-based model order reduction (MOR) technique, has been exercised for local model order reductions. A new efficient process based on the Lagrange interpolation technique has been developed to implement matrix interpolation in the parametric reduced order model (pROM). The reduced order models (ROM) have a degree of freedom (DOF) of just 8, compared to the full-order models' (FOM) of 50,602. The pROM provides an excellent solution and reduces computational time by 84% for the presented case.

Keywords: Model Order Reduction (MOR), Finite Element Method (FEM), Thermal-Mechanical Analysis, Power Electronics Module (PEM), Reliability Assessment, Parametric Model Order Reduction (pMOR)

1. Introduction

Modern technologies are constantly advancing, making engineering projects complex and expensive. Engineers often face challenges in ensuring the reliability and protection of these technologies. Engineering disciplines such as space travel, aeronautics, and nuclear applications require special attention to reliability and safety. Analysts and designers use mathematical models to simulate the working principle of complex physical systems, and these models are highly in demand for reliability assessments.

Nowadays, the most exercised computational method for solving PDEs is the Finite Element Method (FEM). However, FE computing requires complex and extensively high-dimensional systems to be solved. Therefore, to reduce the complexity of the physical problem and its simulation time requirements, the dimensions of these systems must be reduced as a practical computing solution. Modal truncation (Davison, 1966; Grimberg et al., 2020), which delivers adequate approximate models, and Krylov subspace-based model order reduction (MOR) methods are generally used in practice, but Krylov subspace-based approaches are comparatively more automatic (Freund, 2003; Panagiotopoulos et al., 2020).

Thermal behaviours of electronic components have severe effects on their operation and reliability, and thermal-elastic degradation is one of the most important causes of the dissipation of these devices (Choi et al., 2010; Paret et al., 2023). Hence, it is fundamental to carry out coupled thermal-mechanical analysis for reliability assessments of electronic systems.

Using MOR methods for thermal analyses can substantially decrease computation time for reliability predictions. Liu et al. (2012) formed a strategy to utilise the Krylov subspace-based MOR method for simulating the thermal distribution of an AC/DC converter assembly of an EV (Electric Vehicle). Codecasa et al. (2018) presented a MOR-based boundary condition independent (BCI) dynamic compact thermal model (DCTM) fitted to define multiple heat sources examining a PoP (Package on Package) two-die assembly and an IGBT-based power module. Rogié et al. (2018) presented a reduced order model of BCI DCTMs utilising the FANTASTIC matrix reduction code, demonstrating the approach on a single-chip (QFN16) and a dual-chip (DFN12) package. Bissuel et al. (2019) informed a reduced compact model, with the help of the Modal approach and optimization, to simulate the thermal distribution of electronic boards. Codecasa et al. (2020) offered a MOR-based BCI CTM using the FANTASTIC code adept of coupled analysis to the thermal ambient environment and designed a PoP system.

*Correspondings
Email address: s.r.hassan@gre.ac.uk (Sheikh Hassan)

Coupled systems are relatively complex and have higher dimensions, and reduced order modelling approaches are highly regarded to overcome computing requirements. Rajaguru et al. (2020) used Krylov subspace-based MOR techniques to a submodel of an IGBT power electronics module (PEM) for examining stress distribution and thermo-mechanical loading. Rajaguru et al. (2021) described a MOR method to reduce a full order model of an electro-thermal model of wire-bond structures, exhibiting that rational Krylov is comparatively better for such models, and also presented a linear-damage and fatigue analysis.

Parametric studies need a series of simulations as model parameter change is required, and reduced order modelling approaches can significantly decrease its computing time. Feng et al. (2016) examined a multi-moment-matching pMOR approach for thermal and electro-thermal investigation of nanoelectronic structures and further evaluated the automated process of the reduction method. ter Maten et al. (2016) formulated pMOR methods, following the superposition principle, for simulating coupled electromagnetics-heat models. Bouhedma et al. (2020) built a parametric reduced order model via the Arnoldi approach to construct an improved geometry of a Piezoelectric Energy Harvester. Schütz et al. (2021b) carried out a parametric study using three magnetostatic FEM-based models, i.e., a lookup table (LT), a semi-analytical compact model (ACM), and a parametric ROM created using matrix interpolation approach and executed these parametric analysis methods for a control circuit of an electromagnetic system. Yuan et al. (2021) delivered an optimized FE model of a thermoelectric generator and its compact ROM employing multivariate moment-matching and matrix-interpolation-based automatic pMOR approaches.

As nonlinear analysis provides an elaborated detail of a system, it is highly regarded for precise modelling, but the computational time requirements are relatively higher in nonlinear analyses, and reduced order modelling offers a reasonable solution. Schütz et al. (2021a) proposed a process to investigate the FE model of a microsystem architecture with nonlinear input and applied MOR to the model. Scognamillo et al. (2021) performed an electro-thermal study of a power module considering a nonlinear thermal effect and utilising the FANTASTIC tool. Schütz & Bechtold (2023b) presented three numerical scenarios of MEMS micro-actuators, describing the nonlinear behaviour of the system. In the latest research (Hassan et al., 2023a,b), thermal-mechanical PEM models have been considered for parametric studies by parametrising its temperature-dependent wire material properties and examining its nonlinear plasticity behaviours with the pMOR approach.

Most above-referenced MOR and pMOR studies analysed the coupled thermal-mechanical models using the sequential-coupled method. On the other hand, direct-coupled thermal-mechanical modelling approaches are more practical and offer better solutions. Therefore, a direct coupled thermal-mechanical model that can solve both the thermal and mechanical models concurrently has been exercised for the presented work. In addition, prior pMOR investigations mainly focused on parametrising non-temperature-dependent material properties, which do not describe the natural behaviours of materials. Thus, in this parametric study, the temperature-dependent material properties, i.e., coefficient of thermal expansion (CTE) and Young's modulus (E) of aluminium (Al) alloy wire in the PEM have been parametrised. The parametric reduced order model (pROM) has been integrated with the FEM (ANSYS-FEM) to examine the nonlinear plasticity of these wires. For the current pROM, the matrix interpolation method has been implemented with the Krylov subspace-based MOR approach PRIMA. A new matrix interpolation technique based on the Lagrange interpolation method has been developed for the pMOR approach.

2. Mathematical Formulations

2.1. Parametric Full Order Model (pFOM)

The parametric full-order model (pFOM) has a state-space representation that can be expressed as (Panzer et al., 2010; Yuan et al., 2021):

$$\begin{aligned} \boldsymbol{E}(\boldsymbol{p}_i)\dot{\boldsymbol{x}}(\boldsymbol{p}_i,t) &= \boldsymbol{A}(\boldsymbol{p}_i)\boldsymbol{x}(\boldsymbol{p}_i,t) + \boldsymbol{B}(\boldsymbol{p}_i)\boldsymbol{u}(\boldsymbol{p}_i,t) \\ \boldsymbol{y}(\boldsymbol{p}_i,t) &= \boldsymbol{C}(\boldsymbol{p}_i)\boldsymbol{x}(\boldsymbol{p}_i,t) \end{aligned} \tag{1}$$

$\boldsymbol{E}(\boldsymbol{p}_i), \boldsymbol{A}(\boldsymbol{p}_i) \in \mathbb{R}^{N\times N}$ signify system matrices with $\boldsymbol{B}(\boldsymbol{p}_i) \in \mathbb{R}^{N\times M}$ input matrix and $\boldsymbol{C}(\boldsymbol{p}_i) \in \mathbb{R}^{P\times N}$ output matrix and reliant on parametric points, $\boldsymbol{p}_i$. $\boldsymbol{u}(\boldsymbol{p}_i,t) \in \mathbb{R}^M$, $\boldsymbol{y}(\boldsymbol{p}_i,t) \in \mathbb{R}^P$ and $\boldsymbol{x}(\boldsymbol{p_i},t) \in \mathbb{R}^N$ are parametric points, $\boldsymbol{p}_i$, and time, t, dependent inputs, outputs, and states of the system, respectively. $\boldsymbol{p}_i$ represents the vector of parametric points for the model, here $i = 0, 1, \ldots k$ with k indicating the number of design points considered for the study.

2.2. Projection-based Model Order Reduction (MOR)

The local full order model (FOM) of (1), which does not depend on the parametric points ($\boldsymbol{p}_i$), has the state space expression, and can be defined as (Panzer et al., 2010; Yuan et al., 2021):

$$\begin{aligned} \boldsymbol{E}\dot{\boldsymbol{x}}(t) &= \boldsymbol{A}\boldsymbol{x}(t) + \boldsymbol{B}\boldsymbol{u}(t) \\ \boldsymbol{y}(t) &= \boldsymbol{C}\boldsymbol{x}(t) \end{aligned} \tag{2}$$

Here, the system ($\boldsymbol{E}, \boldsymbol{A} \in \mathbb{R}^{N\times N}$), input ($\boldsymbol{B} \in \mathbb{R}^{N\times M}$), and output ($\boldsymbol{C} \in \mathbb{R}^{P\times N}$) matrices do not depend on parametric points ($\boldsymbol{p}_i$). The inputs ($\boldsymbol{u}(t) \in \mathbb{R}^M$), outputs ($\boldsymbol{y}(t) \in \mathbb{R}^P$) and states ($\boldsymbol{x}(t) \in \mathbb{R}^N$) of the system only depend on time (t). $N \in \mathbb{N}$ is the order of the full-order system, and it is substantially high.

Using the model order reduction (MOR) technique, the reduced order model (ROM) of the system in (2) is achievable and can be stated as (Panzer et al., 2010; Yuan et al., 2021):

$$\begin{aligned} \boldsymbol{E}_r\dot{\boldsymbol{x}}_r(t) &= \boldsymbol{A}_r\boldsymbol{x}_r(t) + \boldsymbol{B}_r\boldsymbol{u}_r(t) \\ \boldsymbol{y}_r(t) &= \boldsymbol{C}_r\boldsymbol{x}_r(t) \end{aligned} \tag{3}$$

The reduced matrices in (3) have been attained using the Krylov subspace-based MOR algorithm, PRIMA, and through the subsequent processes: $\boldsymbol{E}_r = \boldsymbol{V}^T\boldsymbol{E}\boldsymbol{V}$, $\boldsymbol{A}_r = \boldsymbol{V}^T\boldsymbol{A}\boldsymbol{V}$, $\boldsymbol{B}_r = \boldsymbol{V}^T\boldsymbol{B}$ and $\boldsymbol{C}_r = \boldsymbol{C}\boldsymbol{V}$ (Odabasioglu et al., 2003; Race et al., 2022). The reduced system matrices, $\boldsymbol{E}_r, \boldsymbol{A}_r \in \mathbb{R}^{q\times q}$, input matrix, $\boldsymbol{B}_r \in \mathbb{R}^{q\times m}$, and output matrix, $\boldsymbol{C}_r \in \mathbb{R}^{p\times q}$, have significantly lower order, i.e., $q \ll N$, and have been realised utilising the transformation matrix $\boldsymbol{V} \in \mathbb{R}^{N\times q}$. The transformation matrix ($\boldsymbol{V}$) has been achieved via the transfer function of the local FOM in (2). The transfer function of the local ROM in (3) is determined per the reduced order matrices. The transfer functions of local FOM in (2) and local ROM (3) can be articulated as (Odabasioglu et al., 2003; Race et al., 2022):

$$\boldsymbol{Y}(s) = \boldsymbol{C}(s\boldsymbol{E} - \boldsymbol{A})^{-1}\boldsymbol{B} \tag{4}$$

$$\boldsymbol{Y}_r(s) = \boldsymbol{C}_r(s\boldsymbol{E}_r - \boldsymbol{A}_r)^{-1}\boldsymbol{B}_r \tag{5}$$

2.3. Interpolation of Sparse Matrices

Considering all the sparse matrices of FOM in (2) as $\boldsymbol{X} = \boldsymbol{E}, \boldsymbol{A}, \boldsymbol{B}$, it is possible to get the state space model in (1) by executing the linear matrix interpolation method as (Panzer et al., 2010; Schütz & Bechtold, 2023a):

$$\boldsymbol{X}(\boldsymbol{p}_i) = \boldsymbol{X}(\boldsymbol{p}_0) + \omega(\boldsymbol{p}_i)\left[\boldsymbol{X}(\boldsymbol{p}_k) - \boldsymbol{X}(\boldsymbol{p}_0)\right] \tag{6}$$

Here, $\omega(\boldsymbol{p}_i)$ is the weighting function, and the values of $\omega(\boldsymbol{p}_i)$ are determined by exercising the linear interpolation method. However, while considering several parametric points for sampling, a multi-linear matrix interpolation method is essential (Hassan et al., 2023a). In this work, $i = 0, 1, ..., k$ and $k = 6$, with three sampled parametric points. A new matrix interpolation technique, previously reported in (Hassan et al., 2023b), based on the Lagrange interpolation method has been implemented for the current investigation, and it can be expressed as:

$$\boldsymbol{X}(\boldsymbol{p}_i) = \omega_0(\boldsymbol{p}_i)\boldsymbol{X}(\boldsymbol{p}_0) + \omega_{\frac{k}{2}}(\boldsymbol{p}_i)\boldsymbol{X}(\boldsymbol{p}_{\frac{k}{2}}) + \omega_k\boldsymbol{X}(\boldsymbol{p}_k) \tag{7}$$

Values of the weighting function, $\omega(\boldsymbol{p}_i)$, are governed using the Lagrange interpolation method.

2.4. Parametric Reduced Order Model (pROM)

A parametric reduced order model (pROM) has been formed using the matrix interpolation technique in (7) with the reduced order modelling approach in (3), and the pROM can be stated as (Panzer et al., 2010; Yuan et al., 2021):

$$\begin{aligned}\boldsymbol{E}_r(\boldsymbol{p}_i)\dot{\boldsymbol{x}}_r(\boldsymbol{p}_i,t) &= \boldsymbol{A}_r(\boldsymbol{p}_i)\boldsymbol{x}_r(\boldsymbol{p}_i,t) + \boldsymbol{B}_r(\boldsymbol{p}_i)\boldsymbol{u}_r(\boldsymbol{p}_i,t)\\ \boldsymbol{y}_r(\boldsymbol{p}_i,t) &= \boldsymbol{C}_r(\boldsymbol{p}_i)\boldsymbol{x}_r(\boldsymbol{p}_i,t)\end{aligned} \tag{8}$$

The generalised trapezoidal rule (GTR), a transient analysis solution method, has been exercised to resolve the pROM established in (8) (Hughes, 2012; ANSYS, 2023). The generalised trapezoidal rule is usually used in FE modelling to perform transient analysis of the state-space model (first order), i.e., (8).

2.5. Parametric Thermal-Mechanical Model

The finite element method (FEM) discretised coupled thermal-mechanical model is a second-order system. The parametric thermal-mechanical model in its state space form can be represented as (Lohmann & Salimbahrami, 2005; ANSYS, 2023):

$$\begin{aligned}\boldsymbol{M}(\boldsymbol{p}_i)\ddot{\boldsymbol{z}}(\boldsymbol{p}_i,t) + \boldsymbol{D}(\boldsymbol{p}_i)\dot{\boldsymbol{z}}(\boldsymbol{p}_i,t) + \boldsymbol{K}(\boldsymbol{p}_i)\boldsymbol{z}(\boldsymbol{p}_i,t)\\ = \boldsymbol{G}(\boldsymbol{p}_i)\boldsymbol{u}(\boldsymbol{p}_i,t)\\ \boldsymbol{y}(\boldsymbol{p}_i,t) = \boldsymbol{L}(\boldsymbol{p}_i)\boldsymbol{z}(\boldsymbol{p}_i,t)\end{aligned} \tag{9}$$

$\boldsymbol{M}(\boldsymbol{p}_i), \boldsymbol{D}(\boldsymbol{p}_i), \boldsymbol{K}(\boldsymbol{p}_i) \in \mathbb{R}^{n\times n}$, $\boldsymbol{G}(\boldsymbol{p}_i) \in \mathbb{R}^{n\times M}$, and $\boldsymbol{L}(\boldsymbol{p}_i) \in \mathbb{R}^{P\times n}$ are mass, damping, stiffness, input, and output matrices, respectively, and the order of this system, n, corresponds to the order of pFOM in (1) as $2n = N$. $\boldsymbol{u}(\boldsymbol{p}_i,t) \in \mathbb{R}^M$, $\boldsymbol{y}(\boldsymbol{p}_i,t) \in \mathbb{R}^P$, and $\boldsymbol{z}(\boldsymbol{p}_i,t) \in \mathbb{R}^n$ are the inputs, outputs, and states of the parametric thermal-mechanical model. The matrices in (9), the parametric thermal-mechanical model, can be further elaborated as (Hughes, 2012; ANSYS, 2023):

$$\begin{aligned}&\boldsymbol{M} = \begin{bmatrix}\boldsymbol{M}_s & \boldsymbol{0}\\ \boldsymbol{0} & \boldsymbol{0}\end{bmatrix}, \boldsymbol{D} = \begin{bmatrix}\boldsymbol{0} & \boldsymbol{0}\\ \boldsymbol{0} & \boldsymbol{D}^t\end{bmatrix}, \boldsymbol{K} = \begin{bmatrix}\boldsymbol{K}_s & \boldsymbol{K}^{ut}\\ \boldsymbol{0} & \boldsymbol{K}^t\end{bmatrix},\\ &\boldsymbol{G} = \begin{bmatrix}\boldsymbol{F}^a\\ \boldsymbol{Q}\end{bmatrix}, \ddot{\boldsymbol{z}} = \begin{bmatrix}\ddot{\boldsymbol{z}}_{ut}\\ \ddot{\boldsymbol{T}}\end{bmatrix}, \dot{\boldsymbol{z}} = \begin{bmatrix}\dot{\boldsymbol{z}}_{ut}\\ \dot{\boldsymbol{T}}\end{bmatrix}, \boldsymbol{z} = \begin{bmatrix}\boldsymbol{z}_{ut}\\ \boldsymbol{T}\end{bmatrix}\end{aligned} \tag{10}$$

$$\text{with,}\quad \boldsymbol{K}^t = \boldsymbol{K}^{tb} + \boldsymbol{K}^{tc} \tag{11}$$

$\boldsymbol{M}_s$ correspond to structural mass matrix. $\boldsymbol{D}^t$ denotes thermal-specific heat matrix. $\boldsymbol{K}_s$, $\boldsymbol{K}^{tu}$ and $\boldsymbol{K}^t$ indicate structural and thermoelastic stiffness and thermal conductivity matrices, respectively, with $\boldsymbol{K}^{tb}$ and $\boldsymbol{K}^{tc}$ representing thermal conductivity matrices of material and convection surfaces. $\boldsymbol{F}^a$ and $\boldsymbol{Q}$ signify mechanical and thermal load vectors. $\boldsymbol{z}_{ut}$ and $\boldsymbol{T}$ are potential displacement and thermal vectors.

The parametric thermal-mechanical model in (9) has been transformed into the parametric state space full order model (pFOM) in (1) as (Lohmann & Salimbahrami, 2005; Hassan et al., 2023a,b):

$$\begin{aligned}&\begin{bmatrix}\boldsymbol{F} & \boldsymbol{0}\\ \boldsymbol{0} & \boldsymbol{M}\end{bmatrix}\begin{bmatrix}\dot{\boldsymbol{z}}\\ \ddot{\boldsymbol{z}}\end{bmatrix} = \begin{bmatrix}\boldsymbol{0} & \boldsymbol{F}\\ -\boldsymbol{K} & -\boldsymbol{D}\end{bmatrix}\begin{bmatrix}\boldsymbol{z}\\ \dot{\boldsymbol{z}}\end{bmatrix} + \begin{bmatrix}\boldsymbol{0}\\ \boldsymbol{G}\end{bmatrix}\boldsymbol{u}\\ &\boldsymbol{y} = \begin{bmatrix}\boldsymbol{L} & \boldsymbol{0}\end{bmatrix}\begin{bmatrix}\boldsymbol{z}\\ \dot{\boldsymbol{z}}\end{bmatrix}\end{aligned} \tag{12}$$

$$\begin{aligned}\text{with,}\quad &\boldsymbol{E} = \begin{bmatrix}\boldsymbol{F} & \boldsymbol{0}\\ \boldsymbol{0} & \boldsymbol{M}\end{bmatrix}, \boldsymbol{A} = \begin{bmatrix}\boldsymbol{0} & \boldsymbol{F}\\ -\boldsymbol{K} & -\boldsymbol{D}\end{bmatrix}, \boldsymbol{B} = \begin{bmatrix}\boldsymbol{0}\\ \boldsymbol{G}\end{bmatrix},\\ &\boldsymbol{C} = \begin{bmatrix}\boldsymbol{L} & \boldsymbol{0}\end{bmatrix}, \dot{\boldsymbol{x}} = \begin{bmatrix}\dot{\boldsymbol{z}}\\ \ddot{\boldsymbol{z}}\end{bmatrix}, \boldsymbol{x} = \begin{bmatrix}\boldsymbol{z}\\ \dot{\boldsymbol{z}}\end{bmatrix}\end{aligned} \tag{13}$$

Here, $\boldsymbol{F} \in \mathbb{R}^{n\times n}$ is an invertible matrix and $\boldsymbol{F} = \boldsymbol{I}_n$ for the considered model. $\boldsymbol{I}_n \in \mathbb{R}^{n\times n}$ depicts an identity matrix.

3. Power Electronics Module (PEM)

For this study, a direct coupled thermal-mechanical investigation of a general two-dimensional power electronics

module (PEM) model has been conducted. The PEM is a *SiC*-based module. The PEM structure utilised for the examination is illustrated in Fig. 1. ANSYS-FEM has been used to construct and discretise the PEM model, and *Al* (alloy) has been considered for the wire material in the PEM structure, parametrising its temperature-dependent material properties with the pMOR approach.

3.1. FEM Model

This study performs a direct coupled and transient thermal-mechanical analysis using the FEM. In the model, *SiC* bodies are imagined as heat sources of the PEM structure. Hence, isothermal boundary conditions have been set to these bodies with a maximum normalised temperature value of $T_{SiC_N} = 1$ (marked as **A** in Fig. 1). The baseplate's (*Cu*) bottom surface is assumed to be exposed to a fluid zone. Therefore, it has a convection boundary condition (Scognamillo et al., 2021). A maximum normalised convection coefficient of $h_{C_N} = 1$ and a maximum normalised ambient temperature of $T_{C_N} = 0.167$ has been set for the convection boundary condition (marked as **C** in Fig. 1). For the mechanical boundary conditions, one vertex in the bottom-left corner and another vertex in the bottom-right corner of the baseplate (*Cu*) (marked as **B** in Fig. 1) are assumed to have no deformations, so fixed support boundary conditions have been applied to these vertices (Xu et al., 2014; Jørgensen et al., 2021). The boundary conditions are set based on widely practised boundary conditions and reported thermal and deformation profiles in the literature. It is a transient simulation with ramped loading steps; this ramped loading is to create an accelerated thermal loading for the power module structure. A total of 10 loading steps have been evaluated for the simulation, as illustrated in Fig. 2, considering varied temperatures and convection coefficients for the heat source and convection surface. Most parameter data are presented in a normalised (non-dimensional) format to present a generalised analysis instead of a problem-specific study. Temperatures and convection coefficients are normalised by dividing their value by the maximum regarded temperature for the heat source (T_{SiC_M}) and the highest convection coefficient (h_{C_M}) deemed for the convection boundary condition, respectively, i.e., $T_{SiC_N} = T_{SiC}/T_{SiC_M}$, $T_{C_N} = T_C/T_{SiC_M}$, and $h_{C_N} = h_C/h_{C_M}$.

Data for material properties have been sourced from the ANSYS booklet by Ashby (2016). The nonlinear plasticity of the wire material, *Al* (alloy), has been modelled with power hardening law, which is based on Gurson's model and is specified as (Gurson, 1977; ANSYS, 2023):

$$\frac{\sigma_Y}{\sigma_0} = \left(\frac{\sigma_Y}{\sigma_0} + \frac{3G}{\sigma_0}\bar{\varepsilon}^p\right)^{N_S} \tag{14}$$

σ_Y and σ_0 represent current and initial yield strengths. G denotes the shear modulus, and N_S represents the stress ratio. $\bar{\varepsilon}^p$ describes microscopic equivalent plastic strain, and it is expressed as (Gurson, 1977; ANSYS, 2023):

$$\dot{\bar{\varepsilon}}^p = \frac{\sigma : \dot{\varepsilon}^p}{(1-f)\sigma_Y} \tag{15}$$

ε^p signifies the microscopic plastic strain tensor, with $\cdot$ denoting its rate change, and σ represents the Cauchy stress tensor, while : corresponds to the inner product between these two tensor variables. f stands for porosity. The values for initial yield strength (i.e., *normalised initial yield strength = initial yield strength/yield strength* = 1.0) and exponent (0.134) have been set following the methods communicated in Wierzbicki (2023); ANSYS (2023).

3.2. Grid Independence Study

A grid independence test has been conducted exploring two different mesh sizes to assess the consistency of the model (Lachance-Barrett & Alexander, 2018). Normalised temperature (T_N) and total deformation data (U_N) along a line in the PEM structure have been reported in Fig. 3 for considered meshes. The results are normalised as: $T_N = T/T_{SiC_M}$, where T is the obtained temperature; $U_N = U/U_M$, where U is the obtained deformation, and U_M is the maximum deformation in the PEM structure for the current case. The considered line for probing these results is a vertical line across the PEM structure covering a wire bond to the baseplate, displayed in Fig 3a. The results show minimal differences in the temperature data, and deformation data has some changes for different mesh sizes, but they still agree well. Mesh 1 consists of $8,843$ nodes and $7,813$ elements, while Mesh 2 includes $5,347$ nodes and $4,539$ elements. Mesh 1 and Mesh 2 have an "outstanding" average orthogonal quality of 0.99, based on the classifications informed by Lachance-Barrett & Alexander (2018); Hassan et al. (2022).

3.3. Parametric Points

The *Al* (alloy) wires in the PEM structure have the properties of temperature-dependent coefficient of thermal expansion (CTE_{Al}) and Young's modulus (E_{Al}). In this work, CTE_{Al} and E_{Al} have been parametrised for the parametric analysis. For the presented parametric analysis, seven uniformly spaced parametric points ($\boldsymbol{p}_i$), shown in Fig. 4, have been taken into consideration to implement pMOR with the matrix interpolation method. So, the temperature-dependent CTE_{Al} and E_{Al} values change uniformly, corresponding to the parametric points. Fig. 5 shows the temperature-dependent CTE_{Al_N} (normalised CTE_{Al}) change according to parametric points, and E_{Al_N} (normalised E_{Al}) values are changed by 0.04 normalised unit for each parametric point. Here, the values are normalised as: $\mathrm{CTE}_{Al_N} = \mathrm{CTE}_{Al}/(2.3 \times 10^{-5}\,{}^{\circ}C^{-1})$, $\mathrm{E}_{Al_N} = \mathrm{E}_{Al}/(\textit{yield strength})_{Al}$, and $T_N = T/T_{SiC_M}$.

3.4. Reduced Model

The parametric full order model (pFOM) in (2) has a total degree of freedom (DOF) of $N = 50,602$, whilst the parametric reduced order model (pROM) in (7) has a total DOF

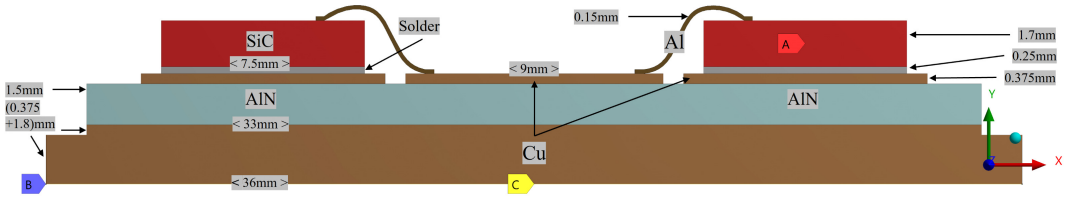

Figure 1: *2D*-plane of the power electronics module structure.

of just $q = 8$. Therefore, the pROM can be computed much faster than the pFOM. On the local level, seven ROMs have been solved for the global parametric reduced order model (pROM), and these local ROMs have been solved during one pROM simulation. On the other hand, for the Full Order Model (FOM), which is the traditional method and uses full order system matrices for calculations, only three local FOMs have been solved for result verification purposes and required time estimation purposes. The pROM required $t_{pROM_N} = 0.16$ normalised time to solve, including the process of order reduction of matrices, compared to pFOM's $t_{pFOM_N} = 1$ normalised time. Simulation times are normalised as: $t_{pFOM_N} = t_{pFOM}/t_{pFOM}$; $t_{pROM_N} = t_{pROM}/t_{pFOM}$, here t_{pFOM} and t_{pROM} are time required for pFOM and pROM to solve. Hence, utilising the pMOR approach, a remarkable 84% reduction in computational time has been achieved. This 84% reduction time includes time for order reduction of system matrices to form the global parametric reduced order model (pROM) and the solution time of this pROM. The compared time is the required time to run the MATLAB code for parametric reduced order modelling processes and reported MAPDL elapsed times in ANSYS, maintaining consistency in the solution procedures.

A flow chart in Fig. 6 summarises the process of creating the pROM with the pMOR approach. The FEM discretisation of the PEM model and the extraction of matrices for three sampled parametric points ($\boldsymbol{p}_0$, $\boldsymbol{p}_3$, and $\boldsymbol{p}_6$) have been done with ANSYS. Then, matrices and MATLAB have been used to develop the pROM per the presented pMOR approach.

3.5. Results and Discussions

Verification of pROM in contrast to pFOM is required to confirm that established pROM is a suitable model. The current thermal-mechanical model's unknowns, i.e., DOFs, are temperature and directional deformations. A

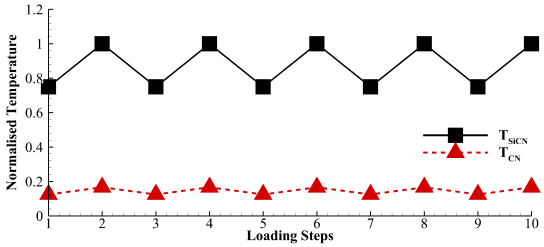

Figure 2: Normalised heat-generating body (T_{SiC_N}) and Ambient temperatures (T_{C_N}) during loading steps.

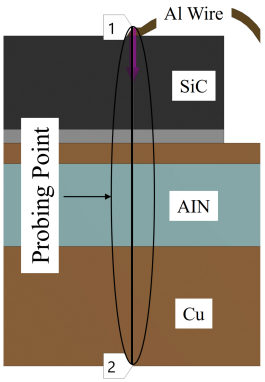

(a) Probing Point (Line/Path).

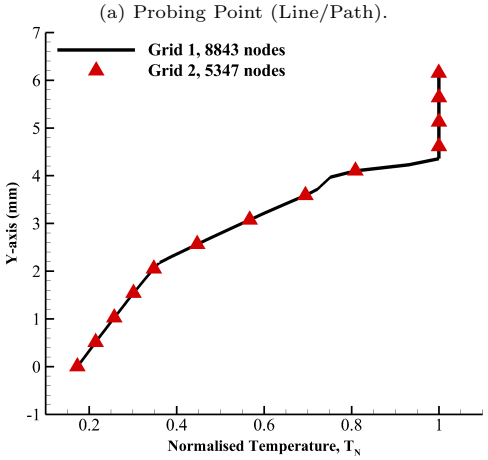

(b) Normalised Temperature, $\boldsymbol{T}_N$.

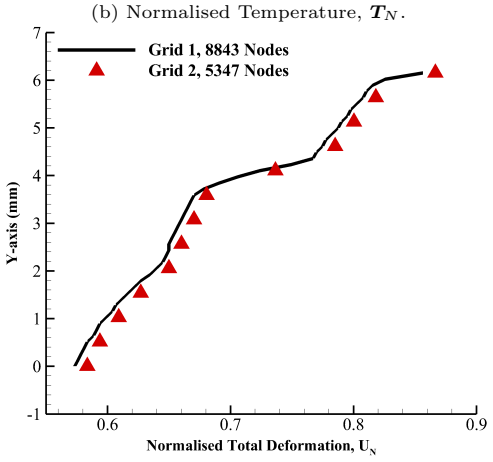

(c) Normalised Total Deformation, U_N.

Figure 3: Mesh sensitivity analysis comparing normalised temperature and normalised total deformation along a probing point (line/path) in the left side of the PEM structure shown in Fig. 1.

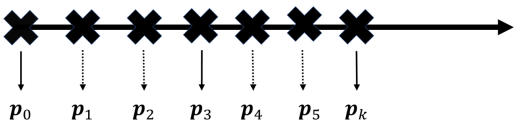

Figure 4: Uniform parametric points.

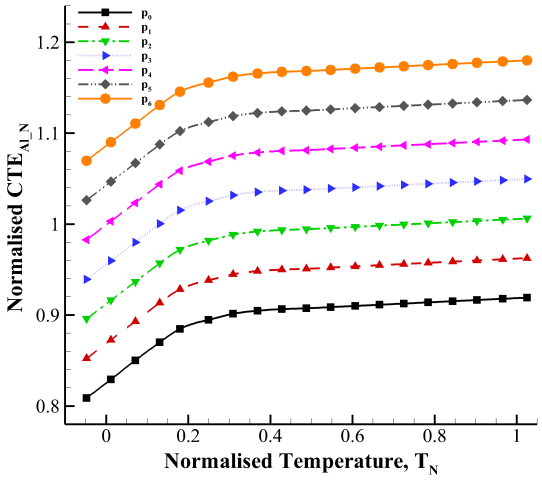

Figure 5: Parametric points for the temperature-dependent normalised coefficient of thermal expansion of Al (alloy), CTE_{Al_N}.

comparative visualisation between pFOM and pROM of the normalised temperature (T_N) and total deformation (U_N) distribution data in the PEM structure has been shown in Fig. 7. Temperature and Total Deformation are normalised as: $T_N = T/T_{SiC_M}$; $U_N = U/U_M$, here, T is the resultant temperature, U and U_M are Total Deformation ovserved and its maximum value. Fig. 7 assesses the outcomes from the parametric point $\boldsymbol{p}_6$. The comparison demonstrates that pROM has been successful in approximating pFOM.

Fig. 7a and 7b shows the temperature distribution in the PEM structure, and it is observed that the wire bond site encounters the highest temperatures, matching with the heat source. The temperature values for the PEM structure have a minimal difference between the pFOM and pROM solutions. Focus has been put on this wire bond site for presenting results.

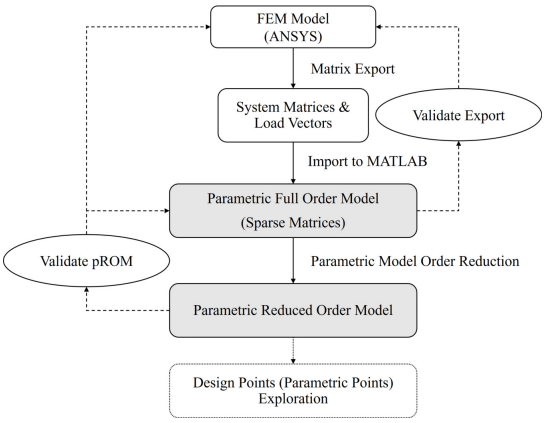

Figure 6: The organizational process to build the pROM.

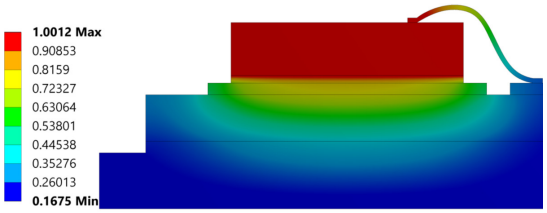

(a) Normalised Temperature, pFOM solution.

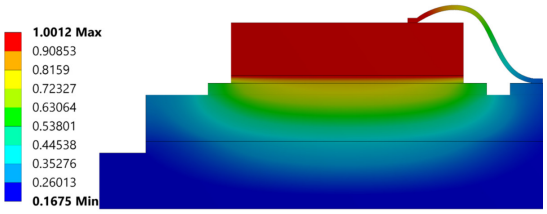

(b) Normalised Temperature, pROM solution.

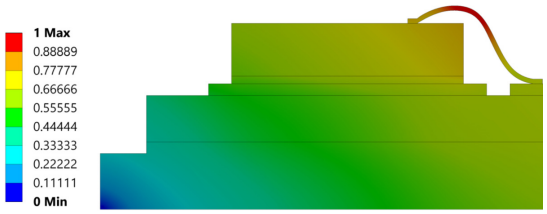

(c) Normalised Total deformation, pFOM solution.

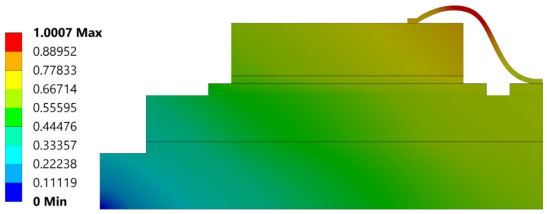

(d) Normalised Total deformation, pROM solution.

Figure 7: Normalised Temperature and Total Deformation distribution from pFOM and pROM solutions in the left part of the PEM structure for the parametric point $\boldsymbol{p}_6$.

The wire in the PEM structure faces the highest deformations, as illustrated in Fig. 7c and 7d, and the wire bond site exhibits notably high deformation distributions. The pROM's total deformation result is in excellent agreement against pFOM, with approximately a 0.1% difference in the peak value. The predicted highest deformation distribution in the wire body is expected.

Fig. 8 demonstrates the normalised equivalent (von-Mises) stresses (σ_{v_N}) around a wire bond site in the PEM structure. Here, $\sigma_{v_N} = \sigma_v/(yield\ strength)_{Al}$, and σ_v is the attained von-Mises stress. pFOM vs pROM solutions can be assessed from Fig. 8a and 8b for the parametric point $\boldsymbol{p}_6$. The stress data establishes that pROM can successfully approximate the outcome of pFOM, and the pMOR method is appropriate for reliability modelling-centred design exploration studies.

Fig. 9 exhibits normalised equivalent (von-Mises) stresses along a line in the wire body. The line in Fig. 9a for probing is in the wire bond site, as it is a significant site for inspection (Nwanoro et al., 2023). Fig. 9b compares stress results obtained from pFOM and pROM

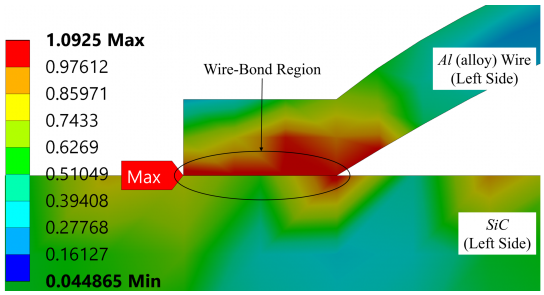

(a) pFOM solution.

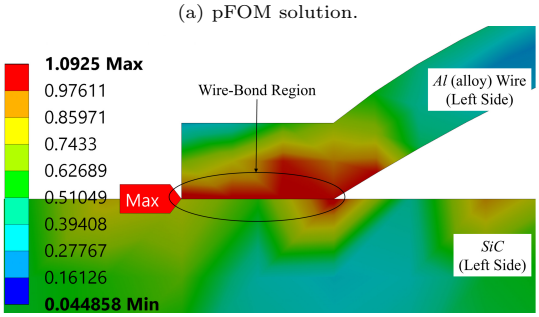

(b) pROM solution.

Figure 8: Normalised Equivalent (von-Mises) stress around the wire bond (left side) of the PEM structure for the parametric point $\boldsymbol{p}_6$.

solutions for the parametric point $\boldsymbol{p}_6$ along the probing point (path/line). The mean difference in the stress results, shown in Fig. 9b, is $< 1\%$ for this considered parametric point. Stress data acquired by the pROM solution for all parametric points have been illustrated in Fig. 9c. It is seen here that normalised stresses are ≥ 1 for all the parametric points, which indicates that these stresses exceed the yield strength of the material, and so permanent damages to the wire bond site are anticipated for studied scenarios.

Fig. 10 compares the contour of normalised equivalent plastic strain (ε_N^p) obtained through pROM and pFOM solutions in the wire body (left side) for the parametric point $\boldsymbol{p}_6$. The plastic strain data are normalised as: $\varepsilon_N^p = \varepsilon^p/\varepsilon_{eq}$; here, ε^p represents occured plastic strain and ε_{eq} is the equivalent total strain observed for corresponding parametric points ($\boldsymbol{p}_i$). The difference between these two results is minor, and pROM can successfully predict a similar outcome as the pFOM. The equivalent plastic strain results represent the degree of work hardening, i.e., inelastic deformation behaviours in the wire material. It is evident from the figure that most of the plastic work occurs in the wire bond region, including maximum plastic strain and this region is most likely to face degradation. The maximum normalised equivalent strain results obtained by the pROM are reported in Table 1 for all considered parametric points. To further verify pROM results, Table 1 also shows the strain results obtained by pFOM for parametric points $\boldsymbol{p}_2$, $\boldsymbol{p}_5$, and $\boldsymbol{p}_6$. It is seen from the table that pROM results have minimal errors compared to the pFOM results. The maximum normalised equivalent strain ranges from 0.1872 for $\boldsymbol{p}_1$ to 0.4061 for $\boldsymbol{p}_6$.

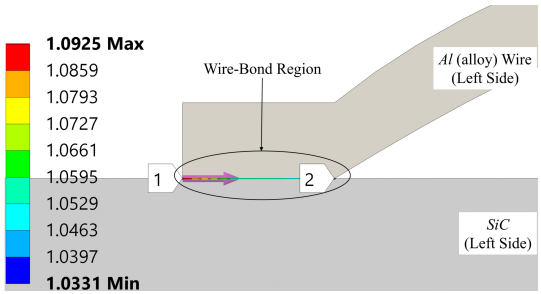

(a) Normalised Equivalent (von-Mises) stress, obtained by the pROM solution, along the probing point (line/path) in the PEM structure for a parametric point $\boldsymbol{p}_6$.

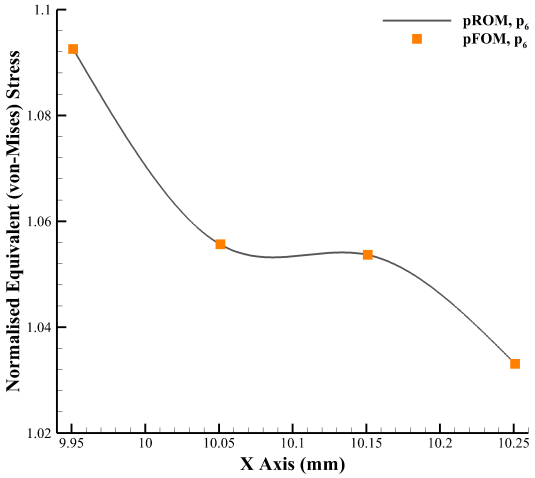

(b) Normalised Equivalent (von-Mises) stress, pFOM vs pROM solution, along the probing point (line/path) in the PEM structure for a parametric point $\boldsymbol{p}_6$.

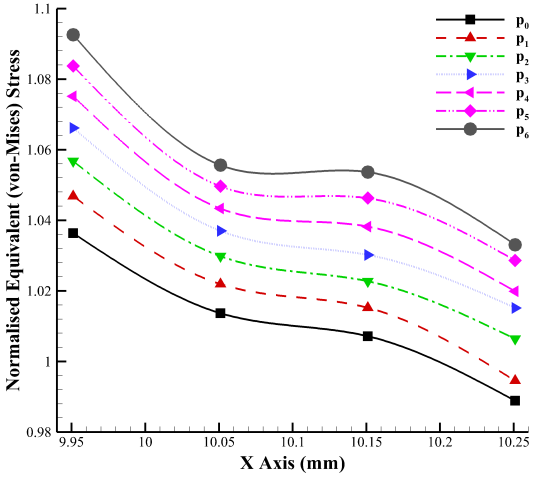

(c) Normalised Equivalent (von-Mises) stressess, obtained by the pROM solution, for all the parametric points.

Figure 9: Normalised Equivalent (von-Mises) stress along a probing point in the wire bond site (in the wire body) of the PEM structure.

3.6. Error Analysis & Optimal Order

The approximate local and parametric reduced-order models in (3) and (8) have some errors corresponding to their full-order models. These errors can be calculated using the transfer functions shown in (4) and (5) as the following (Fehr & Eberhard, 2010; Aumann & Müller, 2023):

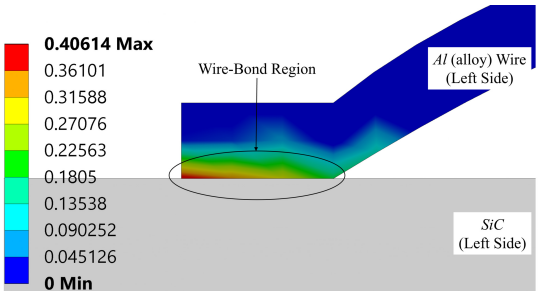

(a) pFOM solution.

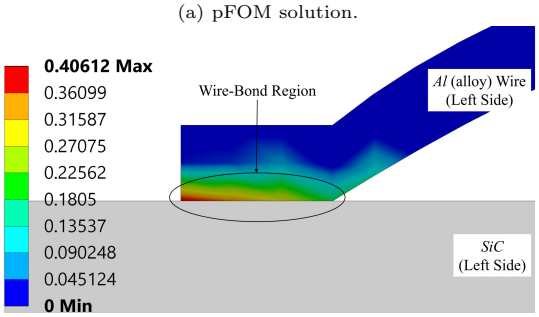

(b) pROM solution.

Figure 10: Normalised Equivalent plastic strain in the wire body (left side) of the PEM structure for the parametric point $\boldsymbol{p}_6$.

Table 1: Maximum normalised equivalent plastic strain in the wire body (left side) of the PEM structure for all the parametric points.

Parametric Points	**Maximum Normalised Equivalent Plastic Strain**	
	pFOM	pROM
$\boldsymbol{p}_0$	–	0.1872
$\boldsymbol{p}_1$	–	0.2338
$\boldsymbol{p}_2$	0.2754	0.2753
$\boldsymbol{p}_3$	–	0.3126
$\boldsymbol{p}_4$	–	0.3461
$\boldsymbol{p}_5$	0.3768	0.3764
$\boldsymbol{p}_6$	0.4061	0.4061

$$\boldsymbol{\epsilon}(\boldsymbol{p}_i, s) = \frac{||\boldsymbol{Y}(\boldsymbol{p}_i,s) - \boldsymbol{Y}_r(\boldsymbol{p}_i,s)||}{||\boldsymbol{Y}(\boldsymbol{p}_i,s)||} \tag{16}$$

The errors in pROM, correlated to the pFOM, have been presented in Table 2 for a considered parametric point ($\boldsymbol{p}_6$). Three reduced order values have been investigated to find an optimal order for the current parametric modelling. The table shows that increasing the reduced-order value from 6 to 8 changes the errors noticeably. However, changing the order of the model to 10 exhibits a slight difference in the errors. Hence, order 8 can be reasoned as the optimal order for the reduced model, and this reduced order has been selected for the presented pMOR study. Additionally, Table 2 compares two MOR algorithms, PRIMA and Arnoldi. In accuracy, both algorithms show similar errors compared to FOM. However, reduced-order modelling with the PRIMA algorithm is more time-efficient. The required time data are normalised as: $t_{ROM_N} = t_{ROM}/t_{FOM}$; here, t_{ROM} represents the time required for reduced-order modelling and t_{FOM} is the time for full-order modelling for the considered parametric point ($\boldsymbol{p}_6$).

Table 2: Error and required normalised time for reduced-order vs. full-order modelling for the parametric point $\boldsymbol{p}_6$.

Order, ROM	**Error, $\boldsymbol{\epsilon}(\boldsymbol{p}_6, s)$**	**Time, t_{ROM_N}**	
	PRIMA or Arnoldi	PRIMA	Arnoldi
6	5.3836×10^{-6}	0.14	0.21
8	2.3627×10^{-6}	0.14	0.25
10	2.1414×10^{-6}	0.18	0.30

4. Conclusion

A general coupled thermal-mechanical model of a power electronics module has been investigated in this work by demonstrating a new way of performing parametric studies and rate-independent non-linear material behaviour analyses of its wires with parametric model order reduction (pMOR) and finite element method (FEM). Temperature-dependent values of the coefficient of thermal expansion and Young's modulus of the wires have been parametrised for the parametric study, and non-linear plasticity behaviours have been studied for the non-linear analysis. The Krylov subspace-based MOR algorithm PRIMA and the matrix interpolation method have been utilised to execute the pMOR approach and achieve the parametric reduced order model (pROM). A new interpolation technique, based on the Lagrange interpolation method, capable of swiftly implementing the matrix interpolation for several sampled parametric points, has been proposed in this work. Presented pROM demonstrated a simulation time reduction of 84% while retaining its prominent level of accuracy compared to its pFOM. The pMOR technique can offer a very efficient and accurate pROM to carry out thermal-mechanical reliability analysis-based parametric studies of large-scale models. The focus of future studies will be on integrating pMOR with FEM (ANSYS-FEM) to study rate-dependent non-linear behaviours of materials in power electronics module structures, which are vital for better reliability assessments.

Declaration of AI-Assisted Technologies

During the preparation of this work, the 1st author used Grammarly to improve the quality of the language in the manuscript. After using this tool, the author reviewed and edited the content as needed and takes full responsibility for the content of the publication.

Acknowledgement

This work was informed by and aligned to the research programmes funded by the UK's EPSRC research council through project grants EP/R004390/1 and EP/W006642/1.

References

ANSYS (2023). Mechanical APDL 2023 R1 - Theory Reference.

Ashby, M. (2016). *Material Property Data for Engineering Materials* volume 27. Cambridge University UK.

Aumann, Q., & Müller, G. (2023). Robust Error Assessment for Reduced Order Vibro-Acoustic Problems. *Journal of Sound and Vibration*, *545*, 117427.

Bissuel, V., Fox, V., Monier-Vinard, E., Neveu, A., Joly, F., & Daniel, O. (2019). Multi-Port Dynamic Compact Thermal Models of BGA Package Using Model Order Reduction and Metaheuristic Optimization. In *2019 18th IEEE Intersociety Conference on Thermal and Thermomechanical Phenomena in Electronic Systems (ITherm)* (pp. 531–539). IEEE.

Bouhedma, S., Rao, Y., Schütz, A., Yuan, C., Hu, S., Lange, F., Bechtold, T., & Hohlfeld, D. (2020). System-Level Model and Simulation of a Frequency-Tunable Vibration Energy Harvester. *Micromachines*, *11*, 91.

Choi, J., Cho, M., & Rhim, J. (2010). Efficient Prediction of the Quality Factors of Micromechanical Resonators. *Journal of Sound and Vibration*, *329*, 84–95.

Codecasa, L., Bornoff, R., Dyson, J., d'Alessandro, V., Magnani, A., & Rinaldi, N. (2018). Versatile MOR-Based Boundary Condition Independent Compact Thermal Models With Multiple Heat Sources. *Microelectronics Reliability*, *87*, 194–205.

Codecasa, L., d'Alessandro, V., & D'Amore, D. (2020). Altering MOR-Based BCI CTMs into Delphi-like BCI CTMs. In *2020 26th International Workshop on Thermal Investigations of ICs and Systems (THERMINIC)* (pp. 97–104). IEEE.

Davison, E. (1966). A Method for Simplifying Linear Dynamic Systems. *IEEE Transactions on automatic control*, *11*, 93–101.

Fehr, J., & Eberhard, P. (2010). Error-Controlled Model Reduction in Flexible Multibody Dynamics. *Journal of Computational and Nonlinear Dynamics*, *5*.

Feng, L., Yue, Y., Banagaaya, N., Meuris, P., Schoenmaker, W., & Benner, P. (2016). Parametric Modeling and Model Order Reduction for (Electro-) Thermal Analysis of Nanoelectronic Structures. *Journal of Mathematics in Industry*, *6*, 1–16.

Freund, R. W. (2003). Model Reduction Methods Based on Krylov Subspaces. *Acta Numerica*, *12*, 267–319.

Grimberg, S., Farhat, C., & Youkilis, N. (2020). On the Stability of Projection-Based Model Order Reduction for Convection-Dominated Llaminar and Turbulent flows. *Journal of Computational Physics*, *419*, 109681.

Gurson, A. L. (1977). *Continuum Theory of Ductile Rupture by Void Nucleation and Growth: Part I—Yield Criteria and Flow Rules for Porous Ductile Media*. Ph.D. thesis Brown University, Providence, R1 (USA). Division of Engineering.

Hassan, S., Akter, U. H., Nag, P., Molla, M., Khan, A., Hasan, M. F. et al. (2022). Large-Eddy Simulation of Airflow and Pollutant Dispersion in a Model Street Canyon Intersection of Dhaka City. *Atmosphere*, *13*, 1028.

Hassan, S., Rajaguru, P., Stoyanov, S., & Bailey, C. (2023a). Parametrising Temperature Dependent Properties in Thermal-Mechanical Analysis of Power Electronics Modules Using Parametric Model Order Reduction. In *2023 46th International Spring Seminar on Electronics Technology (ISSE)* (pp. 1–7). IEEE.

Hassan, S., Rajaguru, P., Stoyanov, S., & Bailey, C. (2023b). Thermal-Mechanical Analysis of a Power Module with Parametric Model Order Reduction. In *2023 24th European Microelectronics & Packaging Conference (EMPC)* (pp. 1–6). IEEE.

Hughes, T. J. (2012). *The Finite Element Method: Linear Static and Dynamic Finite Element Analysis*. Courier Corporation.

Jørgensen, A. B., Munk-Nielsen, S., & Uhrenfeldt, C. (2021). Evaluation of in situ Thermomechanical Stress–Strain in Power Modules Using Laser Displacement Sensors. *IEEE Transactions on Power Electronics*, *36*, 9411–9418.

Lachance-Barrett, S., & Alexander, K. (2018). Wind Turbine Blade FSI (Part 2) — Mesh.

Liu, W., Torsten, H., & Drobnik, J. (2012). Effective Thermal Simulation of Power Electronics in Hybrid and Electric Vehicles. *World Electric Vehicle Journal*, *5*, 574–580.

Lohmann, B., & Salimbahrami, B. (2005). Reduction of Second Order Systems using Second Order Krylov Subspaces. *IFAC Proceedings Volumes*, *38*, 614–619.

ter Maten, E. J. W., Putek, P. A., Günther, M., Pulch, R., Tischendorf, C., Strohm, C., Schoenmaker, W., Meuris, P., De Smedt, B., Benner, P. et al. (2016). Nanoelectronic COupled Problems Solutions-nanoCOPS: Modelling, Multirate, Model Order Reduction, Uncertainty Quantification, Fast Fault Simulation. *Journal of Mathematics in Industry*, *7*, 1–19.

Nwanoro, K. C., Lu, H., Yin, C., & Bailey, C. (2023). Advantages of the Extended Finite Element Method for the Analysis of Crack Propagation in Power Modules. *Power Electronic Devices and Components*, *4*, 100027.

Odabasioglu, A., Celik, M., & Pileggi, L. T. (2003). PRIMA: Passive Reduced-Order Interconnect Macromodeling Algorithm. *The Best of ICCAD: 20 Years of Excellence in Computer-Aided Design*, (pp. 433–450).

Panagiotopoulos, D., Deckers, E., & Desmet, W. (2020). Krylov Subspaces Recycling Based Model Order Reduction for Acoustic BEM Systems and an Error Estimator. *Computer Methods in Applied Mechanics and Engineering*, *359*, 112755.

Panzer, H., Mohring, J., Eid, R., & Lohmann, B. (2010). Parametric Model Order Reduction by Matrix Interpolation. *Automatisierungstechnik*, *58*, 475–484.

Paret, P., Glaws, A., Moreno, G., Major, J., Khan, F., & Narumanchi, S. (2023). Automated Design-for-Reliability of a Power Electronics Module. In *2023 22nd IEEE Intersociety Conference on Thermal and Thermomechanical Phenomena in Electronic Systems (ITherm)* (pp. 1–6). IEEE.

Race, S., Philipp, A., Nagel, M., Ziemann, T., Kovacevic-Badstuebner, I., & Grossner, U. (2022). Circuit-Based Electrothermal Modeling of SiC Power Modules with Nonlinear Thermal Models. *IEEE Transactions on Power Electronics*, *37*, 7965–7976.

Rajaguru, P., Bella, M., & Bailey, C. (2021). Applying Model Order Reduction to the Reliability Prediction of Power Electronic Module Wirebond Structure. In *2021 27th International Workshop on Thermal Investigations of ICs and Systems (THERMINIC)* (pp. 1–6). IEEE.

Rajaguru, P., Lu, H., Bailey, C., & Bella, M. (2020). Modelling and Analysis of Vibration on Power Electronic Module Structure and Application of Model Order Reduction. *Microelectronics Reliability*, *110*, 113697.

Rogié, B., Codecasa, L., Monier-Vinard, E., Bissuel, V., Laraqi, N., Daniel, O., D'Amore, D., Magnani, A., d'Alessandro, V., & Rinaldi, N. (2018). Multi-Port Dynamic Compact Thermal Models of Dual-Chip Package Using Model Order Reduction and Metaheuristic Optimization. *Microelectronics Reliability*, *87*, 222–231.

Schütz, A., & Bechtold, T. (2023a). Matrix Interpolation-Based Parametric Model Order Reduction of Electromagnetic Systems with Translational Movement. In *2023 24th International Conference on Thermal, Mechanical and Multi-Physics Simulation and Experiments in Microelectronics and Microsystems (EuroSimE)* (pp. 1–6). IEEE.

Schütz, A., & Bechtold, T. (2023b). Model Order Reduction of Microactuators: Theory and Application. *Actuators*, *12*, 235.

Schütz, A., Maeter, S., & Bechtold, T. (2021a). System-Level Modelling and Simulation of a Multiphysical Kick and Catch Actuator System. *Actuators*, *10*, 279.

Schütz, A., Olbrich, M., Hu, S., Ament, C., & Bechtold, T. (2021b). Parametric System-Level Models for Position-Control of Novel Electromagnetic Free Flight Microactuator. *Microelectronics Reliability*, *119*, 114062.

Scognamillo, C., Catalano, A. P., Riccio, M., d'Alessandro, V., Codecasa, L., Borghese, A., Tripathi, R. N., Castellazzi, A., Breglio, G., & Irace, A. (2021). Compact Modeling of a 3.3 kV SiC MOSFET Power Module for Detailed Circuit-Level Electrothermal Simulations Including Parasitics. *Energies*, *14*, 4683.

Wierzbicki, T. (2023). *Structural Mechanics (Wierzbicki)*. Massachusetts Institute of Technology via MIT OpenCourseWare. https://eng.libretexts.org (Accessed 2023-July).

Xu, L., Liu, Y., & Liu, S. (2014). Modeling and Simulation of Power Electronic Modules with Microchannel Coolers for Thermo-Mechanical Performance. *Microelectronics reliability*, *54*, 2824–2835.

Yuan, C., Hohlfeld, D., & Bechtold, T. (2021). Design Optimization of a Miniaturized Thermoelectric Generator via Parametric Model Order Reduction. *Microelectronics Reliability*, *119*, 114075.